High-resolution KMM radiative Auger x-ray emission spectra of calcium induced by synchrotron radiation

W. Cao, M. Kavčič, J.-Cl. Dousse, M. Berset, K. Bučar, M. Budnar, K. Fennane, J. Hoszowska, Y.-P. Maillard, J. Szlachetko, M. Szlachetko, and M. Žitnik

Phys. Rev. A **83**, 042513 — Published 20 April 2011

DOI: 10.1103/PhysRevA.83.042513

High-resolution KMM radiative Auger x-ray emission spectra of calcium induced by synchrotron radiation

W. Cao[1],* M. Kavčič[2], J.-Cl. Dousse[1], M. Berset[1], K. Bučar[2], M. Budnar,[2], K. Fennane[1], J. Hoszowska[1], Y.-P. Maillard[1], J. Szlachetko[3,4], M. Szlachetko[1], and M. Žitnik[2]

[1]*Department of Physics, University of Fribourg, Ch. du Musée 3, Ch-1700 Fribourg, Switzerland*

[2]*J. Stefan Institute, P.O. Box 3000, SI-1001 Ljubljana, Slovenia*

[3]*Swiss Light Source, Paul Scherrer Institute, 5232 Villigen, Switzerland and*

[4]*Institute of Physics, Jan Kochanowski University, 25-406 Kielce, Poland*

Abstract

The KMM radiative Auger (RA) x-ray spectra of solid Ca were induced by monochromatic synchrotron radiation and measured with a high-resolution von Hamos bent crystal spectrometer. Two excitation energies were employed, one in the near K threshold region and the second well above the K absorption edge. The KMM RA spectral structure and relative intensity with respect to the diagram $K\beta_{1,3}$ ($K - M_{3,2}$) line are found to be independent of the excitation energy. The overall RA structure resembles the density of unoccupied s-, p- and d- states. Due to solid state effects, however, spectral features resulting from the major discrete shake-up transitions could not be resolved. For the total KMM RA to $K\beta_{1,3}$ yield ratio, a value of 0.053(3) is obtained. The latter is compared to theoretical predictions and available experimental data obtained by various types of target excitation.

PACS numbers: 32.30.Rj, 32.70.Fw, 32.80.Hd

* wei.cao@unifr.ch, wei.cao@usask.ca; Present address: Department of Chemistry, University of Saskatchewan, 110 Science Place, Saskatoon, S7N 5C9 SK, Canada.

I. INTRODUCTION

The decay scheme of atomic inner-shell vacancies is dominated by radiative (fluorescence) and non-radiative (Auger) electron transitions. The radiative Auger effect (RAE) represents an additional decay channel in which a photon and an electron are emitted simultaneously, sharing the available transition energy. This alternative weak deexcitation channel was predicted by Bloch and co-workers already in the 1930s [1, 2] and observed by Åberg and Utriainen only about 35 years later [3].

For the most probable RA transitions, the K–MM ones, which are addressed in this work, the energy E of the emitted photon is given by

$$E = E[K^{-1}] - E[M^{-1}M^{-1}(nl, \epsilon l)], \tag{1}$$

where the first term on the right represents the total energy of an ion with a single hole in the K-shell and the second one the total energy of the final configuration state with two holes in the M-shell and one electron either in an unoccupied bound state nl (shake-up) or in the continuum with an energy ϵ (shake-off). The energy distribution of the RA photons is continuous from zero up to a maximum value which corresponds to the onset of the RA transition. The photon energy is equal to the onset energy when the electron is emitted with a kinetic energy ϵ=0, whereas $E = 0$ when the kinetic energy of the RA electron is equal to the energy of the electron emitted by the parent K–MM Auger transition, i.e., when

$$\epsilon = E[K^{-1}] - E[M^{-1}M^{-1}]. \tag{2}$$

The energy of the $K\beta_{1,3}$ diagram line (K–$M_{3,2}$ transition) can be written similarly as

$$E(K\beta_{1,3}) = E[K^{-1}] - E[M_{3,2}^{-1}], \tag{3}$$

where $E[M_{3,2}^{-1}]$ stands for the total energy of the ion with one vacancy in the M_3 or M_2 subshell. The x-ray emission corresponding to the K–MM RAE appears therefore on the low-energy side of the $K\beta_{1,3}$ x-ray line with a negative energy offset given by

$$\triangle E = E[M_{3,2}^{-1}] - E[M^{-1}M^{-1}(nl, \epsilon l)]. \tag{4}$$

The smallest RA SU (shake-up) energy offset occurs when nl corresponds to the lowest unoccupied state, while the smallest energy offset of a RA SO (shake-off) transition corresponds

to $\epsilon \approx 0$, i.e., to

$$\triangle E \approx E[M_{3,2}^{-1}] - E[M^{-1}M^{-1}]. \tag{5}$$

In RA SO transitions the energy sharing between the continuum electron and the photon is strongly asymmetric [4]. The transition probability is maximum when the electron energy $\epsilon \approx 0$ and the probability diminishes then continuously with ϵ.

Since in RA transitions the energy is shared between the photon and the electron which is shaken off or excited into one of the higher unoccupied states, RA x-ray emission spectra should reflect the structure of the unoccupied states. Indeed, it was shown by Kawai that the shapes of $KL_{2,3}L_{2,3}$ RA x-ray spectra resemble those of K x-ray absorption near edge structure (XANES) spectra. Taking advantage of these similarities, Kawai developed a novel technique for material analysis [5]. This so-called extended x-ray emission fine structure (EXEFS) technique was successfully applied to study the electronic structure of several elements and compounds [6].

Regarding the intensity of the RA x-ray yield relative to the parent diagram line, a decrease with the atomic number Z is predicted by theory [7, 8]. On the other hand, for a given initial inner-shell vacancy, the relative RA x-ray emission yield increases with the principal quantum number of the electrons involved in the transition because of the higher shake probability characterizing the less bound outer shell electrons. However, large discrepancies exist between the existing experimental data and the available shake-off (up) [7], configuration interaction (CI) [9], DV-X_α [10], and radiative field [11, 12] calculations for the relative intensities as well as for the RA x-ray emission spectral shapes.

Within the RAE spectral region other processes such as the radiative electron rearrangement (RER) [13–16] may contribute to the overall signal. The same holds for satellite and hypersatellite x-ray lines due to multiple ionization processes. The contribution from the multiple ionization, which depends on the incident photon energy [17–19], can be reduced by using synchrotron radiation and tuning the excitation energy just above the ionization threshold. For near-threshold excitation energies, however, the RAE signal may then also partially overlap with x-ray resonant Raman structures [20].

Since the RAE transitions are much less intense than their parent diagram x-ray lines and are sitting on the low energy tails of the latter, the RA x-ray spectra are usually measured by means of the wavelength dispersive x-ray spectroscopy technique. To date, experiments based on photoexcitation employing x-ray tubes [21–23] or charged particle excitation [24, 25]

have been carried out. In these studies the contribution of the multiple ionization to the x-ray yield observed within the RA spectral region could not be excluded.

In the present work we report on the KMM RA transitions of Ca induced by monochromatic synchrotron radiation (SR). KMM RA transitions which appear on the low energy tail of the $K\beta_{1,3}$ diagram line were chosen because they are the strongest radiative Auger transitions decaying K-shell vacancies. For the choice of the target, preference was given to Ca because for this element different theoretical predictions for the KMM RAE yields were available [8, 12]. On the other hand, among the few existing experimental data concerning the KMM RA transitions of Ca, none of them was obtained using SR for the target excitation. Present RAE results were obtained with SR beams whose energies were tuned 50 eV and 1455 eV above the K absorption edge. In order to evaluate accurately the background underlying the RA x-ray emission signal, a broad spectral region comprising the $K\alpha_{1,2}$ (K–$L_{3,2}$) and $K\beta_{1,3}$ diagram lines was collected. To extract properly the RA x-ray emission spectral structure and determine in a reliable way the relative RA yield the whole K x-ray spectrum was fitted.

II. EXPERIMENT

The measurements were carried out at the x-ray microscopy beamline ID21 of the European Synchrotron Radiation Facility (ESRF), in Grenoble, France. The primary x-ray beam from the undulator was monochromatized by means of a double-crystal Si(111) monochromator and the higher harmonics were strongly reduced by means of a Ni-coated mirror. The relative beam energy resolution was $\sim 2 \times 10^{-4}$. The beam energies were calibrated by measuring the K-absorption edges of Ca, Sc, Ti and V, using for the edge energies the values reported in Ref. [26]. Two calcium foils, one for the measurement of the absorption edge and another one for the measurements of the emission spectra, were prepared beforehand in Fribourg and transported in vacuum to the ESRF.

The calcium K-edge absorption spectrum was measured in the fluorescence mode in the energy interval of 4017 eV to 4135 eV. For the x-ray emission measurements, a von Hamos curved crystal spectrometer [27] was installed in the main experimental hutch of ID21, downstream of the scanning x-ray microscope chamber to which it was connected with a 180 cm long evacuated pipe sealed with a 50 μm thick Kapton$^{\mathbf{TM}}$ foil. In most applications

the von Hamos spectrometer of Fribourg is operated in the so-called slit geometry. In this geometry a narrow rectangular slit, placed between the target and the bent crystal, serves as the effective source of radiation and the energy resolution of the spectrometer is mainly determined by the chosen width of the slit. It can be noted that, due to the slit, different parts of the reflecting area of the crystal view different parts of the target so that the shape of the measured x-ray spectrum has to be corrected off-line for spatial inhomogeneities of the beam intensity on the target. In the present experiment, however, in order to maximize the intensity of the fluorescence x rays impinging on the crystal and to get rid of the dependence of the x-ray spectrum shape on the inhomogeneous beam intensity profile, a 200 μm pinhole was inserted in the primary beam and the slit of the spectrometer was left completely open. In this "slitless" mode of operation, the energy resolution of the von Hamos spectrometer depends primarily on the size (width) of the beam on the target. With the chosen pinhole diameter the FWHM instrumental broadening of the spectrometer was $\sim$ 1.6 eV for the energy region corresponding to the KMM RA spectrum of Ca.

A top view of the experimental setup is shown in Fig. 1. The 5.1 mg/cm^2-thick Ca foil was mounted perpendicularly to the incoming beam. The emitted photons were diffracted in first order by a LiF(200) crystal, bent cylindrically to a radius R = 25.4 cm. For the detection of the diffracted photons a thermoelectrically cooled (-50 °C) back-illuminated CCD camera consisting of 1340×400 pixels with a pixel size of 20×20 μm^2 was used. Depending on the central Bragg angle θ, the detector covered an energy range varying from 83 eV to 97 eV. Thus, to record the whole RA spectrum together with the $K\alpha_{1,2}$ and $K\beta_{1,3}$ diagram lines, four different detector positions were required. In order to ensure the normalization of the x-ray spectra measured at different detector positions, the latter were chosen so that there was an overlap of $\sim 20 - 30$ eV between neighboring spectra.

By setting appropriate energy windows, the CCD detector allows discrimination against higher-order crystal reflections and also a rejection of background events, provided that there are no multiple hits on the CCD pixels. In order to avoid multiple photon absorption within a single pixel, acquisition times of 1s/image were chosen for the measurements of the intense diagram lines and the intensity of the incoming photons was attenuated by inserting thin absorbers in the beam (a 25 μm-thick Ti foil for the $K\alpha_{1,2}$ measurements and a 90 μm-thick Al foil for the $K\beta_{1,3}$ ones). For the measurement of the weak RA spectrum no absorber was used and the exposure times were 1s/image for the part of the spectrum lying close to

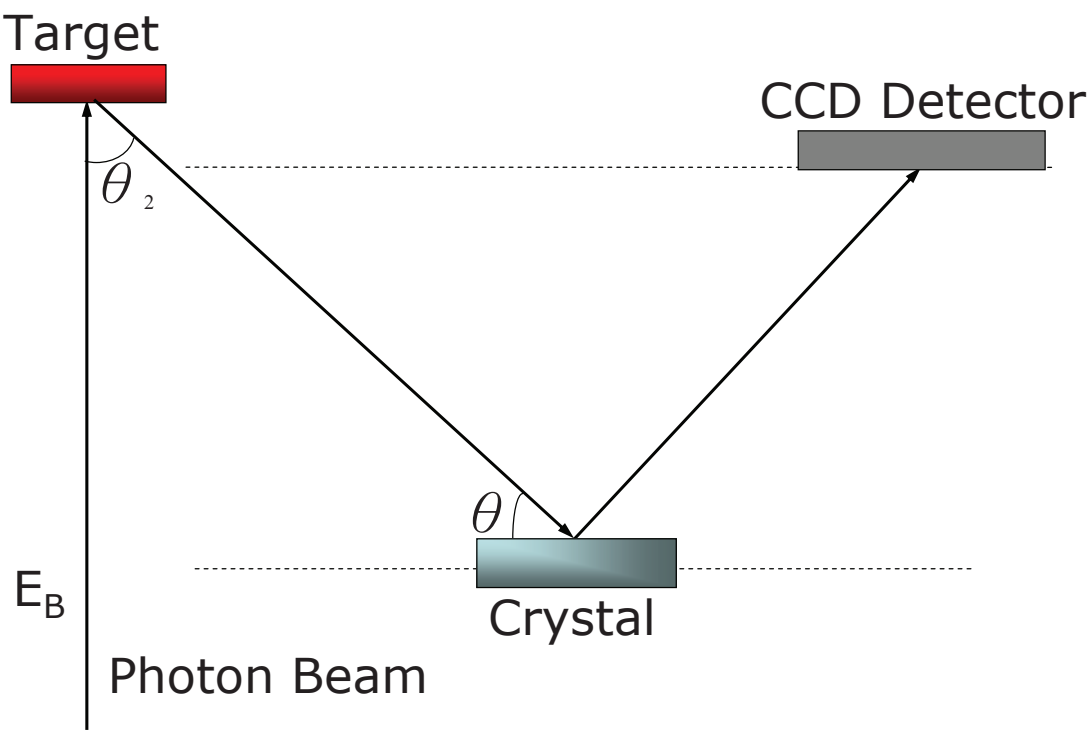

FIG. 1. (Color online) Top view of the experimental set-up used in this work (see text for further details).

the $K\beta_{1,3}$ line and 2s/image for the rest of the spectrum. For normalization purposes, the incident photon fluxes were recorded with a photodiode before and after each measurement. The incident photon flux without absorbers was typically $3 - 6 \times 10^{11}$ photons/s.

The incident photon beam energy was tuned to 4088 eV, an energy lying above the K absorption edge of Ca (4038.2 eV) but clearly below the KL and KK double ionization thresholds. In addition, the difference of 50 eV between the beam energy and the K edge allowed us to avoid a contamination of the RAE energy region by the KM resonant Raman scattering. The RAE measurements were also performed using a higher beam energy of 5493 eV, which is above the KL double ionization threshold. The aims of the latter measurements were to check the effect of multiple ionization and to probe the dependence of the RA process on the incoming photon energy. To obtain data with a good statistics, an acquisition time

of ~ 8 hours was needed for a whole RA spectrum. At each beam energy, the spectrometer was calibrated using the known energy of the elastic peak scattered by thin metallic Ti and V foils and the calcium $K\alpha_1$ transition energy quoted in Ref. [26]. These measurements also served to determine the instrumental broadening of the spectrometer.

III. DATA ANALYSIS

A. Data corrections

The measured x-ray intensities $I_{exp}(E)$ were first normalized by the photon flux and the overall acquisition time. They were then corrected for the target self-absorption (correction factor F_{SA}), the CCD quantum efficiency ($F_{\mathbf{CCD}}$), the crystal reflectivity (F_{CR}), and the solid angle of the spectrometer (Ω), using the relation

$$I(E) = \frac{I_{exp}(E)F_{SA}(E)}{\Omega(E)F_{\mathbf{CCD}}(E)F_{CR}(E)}. \tag{6}$$

For the self-absorption correction, the following equation was used

$$F_{SA}(E) = \frac{[\mu_B/\cos\theta_1 + \mu(E)/\cos\theta_2]t}{1 - \exp[-(\mu_B/\cos\theta_1 + \mu(E)/\cos\theta_2)t]}, \tag{7}$$

where t represents the target thickness, θ_1 and θ_2 are the angles of the incident and fluorescence photon beams with respect to the normal to the sample surface, and μ_B and $\mu(E)$ stand for the attenuation coefficients at the incident-beam energy E_B and x-ray emission energy E, respectively. Note that in the present experimental setup, $\theta_1 = 0^{\mathbf{o}}$ so that $\cos\theta_1 = 1$ and $\cos\theta_2 = \sin\theta$, where θ is the Bragg angle (see Fig. 1).

The attenuation coefficients μ_B corresponding to the two beam energies were derived from the theoretical values reported in Ref. [28], while the function $\mu(E)$ was calculated using the analytical power-law [29, 30]

$$\mu(E) = aE^b. \tag{8}$$

The parameters a and b were determined by fitting the above function to the values quoted in Ref. [28] for the K pre-edge energy region.

Although the major part of the measured x-ray emission spectrum, including the whole RA structure of primary interest, lies below the K absorption edge, the high energy part of

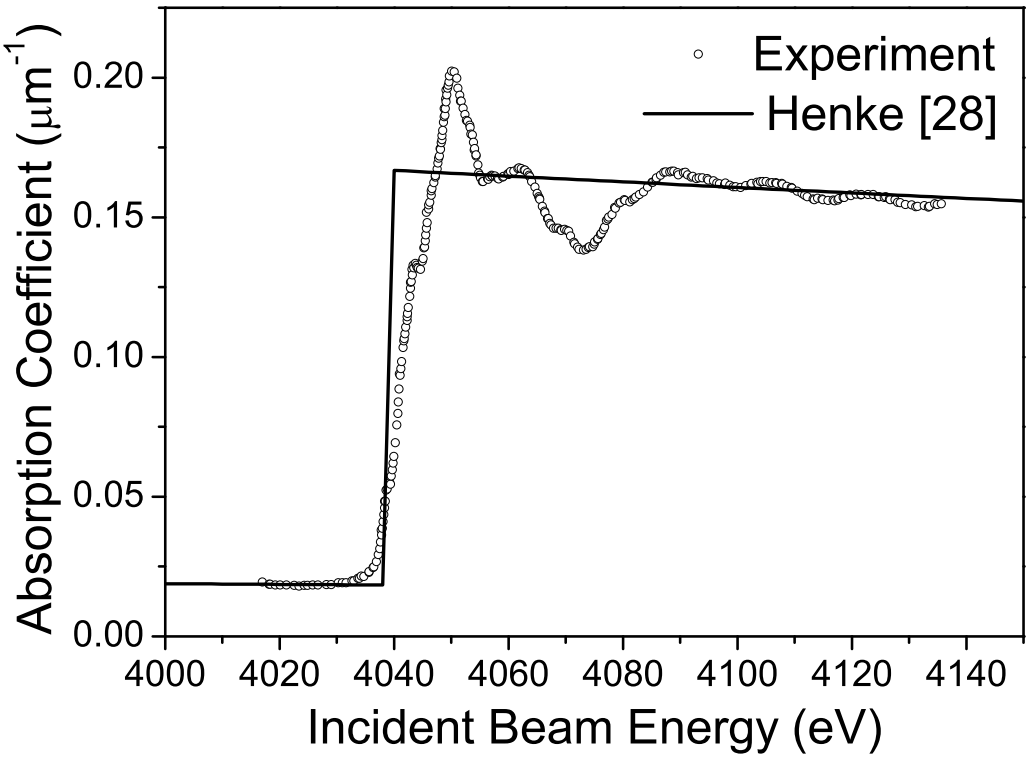

FIG. 2. Experimental (open circles) and theoretical (solid line) [28] x-ray absorption coefficients for solid calcium. Note that the absorption coefficients are expressed in $\mu\mathrm{m}^{-1}$.

the spectrum above the $K\beta$ diagram line, particularly the $K\beta_5$ ($K - M_{4,5}$) line, is affected by an increased self-absorption due to the vicinity of the K absorption edge. In order to avoid the use of a step-like function for the absorption edge [28], the data from the measured absorption spectrum were used for the correction factor $F_{SA}(E)$. To get the experimental x-ray attenuation coefficients, the absorption spectrum was rescaled above the K XANES region to the theoretical data from [28]. The result of this rescaling procedure, depicted in Fig. 2, exhibits a good general agreement between our measured absorption spectrum and the theoretical values. The so-obtained experimental attenuation coefficients were then used to calculate the $F_{SA}(E)$ correction factors in the near K absorption edge region.

The energy dependent efficiency $F_{\mathbf{CCD}}(E)$ of the back-illuminated silicon CCD detector

was determined using the following relation from [31]

$$F_{\mathbf{CCD}}(E) = C_D \left[1 - \exp(-\frac{10^6 X_{Si}}{6.67(1+\frac{E}{1000})^{3.14615}}) \right], \quad (9)$$

where C_D is a dimensionless constant, X_{Si} the effective thickness in cm of the CCD Si layer, and E the energy of the detected x-rays in eV. For the back-illuminated CCD camera used in the present experiment, the constant C_D is nearly equal to 1 and the thickness X_{Si} amounts to $\sim$0.0015 cm [32]. The reflectivity of the LiF(200) crystal was calculated by means of the XOP program [33] for eight energies between the $K\alpha_{1,2}$ and $K\beta_{1,3}$ lines and then fitted with a 2nd-order polynomial to obtain the reflectivity correction function $F_{CR}(E)$. Finally, the smooth variation with energy of the solid angle $\Omega(E)$ was determined using a dedicated computer code.

B. Spectra fitting

The high-resolution Ca K x-ray spectra corresponding to the two beam energies are presented in Fig. 3. Both spectra are dominated by the strong $K\alpha_{1,2}$ and $K\beta_{1,3}$ diagram lines with the broad RA structure of interest between them. On the high energy side of the $K\beta_{1,3}$ line one can also see the weak quadrupole-allowed $K\beta_5$ line ($K - M_{4,5}$ transition). Furthermore, as shown in Fig. 3, the L satellites of the $K\alpha_{1,2}$ and $K\beta_{1,3}$ x-ray lines are only observed in the spectrum measured at the higher beam energy. This is, however, not surprising since the first beam energy (4088 eV) was smaller than the KL double ionization threshold.

For a reliable analysis of the measured x-ray spectra one should consider that the diagram transitions may be accompanied by satellite transitions. The latter result from the presence of additional vacancies in the outer subshells that are produced mainly by shake processes [34]. Due to these spectator vacancies the screening of the nuclear charge is reduced and the x-ray satellite lines are shifted in energy with respect to the diagram transitions. Multiconfiguration Dirac-Fock (MCDF) calculations [35] show that the first-order N-satellites are not resolved from the $K\alpha_{1,2}$ and $K\beta_{1,3}$ diagram lines. This overlap of the N satellites with their parent diagram lines leads to a non-lifetime broadening of the latter. For the first-order M-satellites the energy shifts are somewhat bigger but not enough to separate them from their parent diagram lines. In this case the satellites make the diagram lines

asymmetric. In contrast to N and M satellites, the $K\alpha_{1,2}L$ and $K\beta_{1,3}L$ satellite transitions whose average energies are ∼24 eV and ∼46 eV above their parent diagram transitions can be well resolved (see Fig. 3b).

The normalized and corrected x-ray spectra were analysed with the least-squares fit program Peakfit$^{\mathbf{TM}}$. In the spectrum measured at 4088 eV a small asymmetry was observed for the $K\alpha_{1,2}$ diagram line. Although the beam energy was lower than the KL double ionization threshold, it was high enough to induce KN and KM double excitations/ionizations. Thus, the $K\alpha_{1,2}$ lines were fitted with four Voigtians, two for the diagram lines and two for the unresolved N plus M satellite structures. The same Gaussian width corresponding to the known instrumental broadening was used for each Voigtian. The Lorentzian widths of the Voigtians corresponding to the diagram lines were deduced from the recommended atomic level widths reported by Campbell and Papp [36] and kept fixed in the fit, whereas the Lorentzian widths of the Voigtians used to fit the M plus N satellites were taken as free fitting parameters. The centroid energies and intensities of the Voigtians as well as the parameters of the linear background were also let free in the fit. For the $K\beta_{1,3}$ x-ray lines, a similar fitting procedure was employed but the Lorentzian widths of the diagram lines were left free due to the higher uncertainties of the M-shell widths resulting from the strong overlap between the $M_{2,3}$ and $M_{4,5}$ levels [37]. The weak $K\beta_5$ transition was fitted with a single Voigtian, all parameters being let free in the fit except the Gaussian width. The total fit to the spectrum and the individual peak components are plotted in Fig. 3(a) in a logarithmic scale in order to emphasize the weak structures.

The spectrum recorded at the higher beam energy (E_B=5493 eV) was analyzed in a similar way (see Fig. 3(b)). However, the diagram lines were found to exhibit a larger asymmetry due to the increased intensities of the unresolved M- and N-satellites. For the $K\beta_{1,3}$ line the asymmetry being more pronounced, an additional Voigtian had to be used in the fit. Furthermore, as in this case the beam energy was higher than the KL double ionization threshold, additional peaks were needed to account for the resolved $K\alpha_{1,2}L$ and $K\beta_{1,3}L$ satellite lines. From the fit, energy shifts of 23.8(2) eV and 46.6(3.8) eV were obtained for the $K\alpha_1 L$ and $K\beta_{1,3}L$ satellites relatively to their parent diagram lines. The first result is slightly bigger than the values of 22.4(8) eV and 22(2) eV reported by Oura et al. [38] and Deutsch [39], respectively, whereas the second result is in good agreement with the theoretical value of 48.7 eV calculated with the GRASP code [35]. For the $K\beta_5$ to

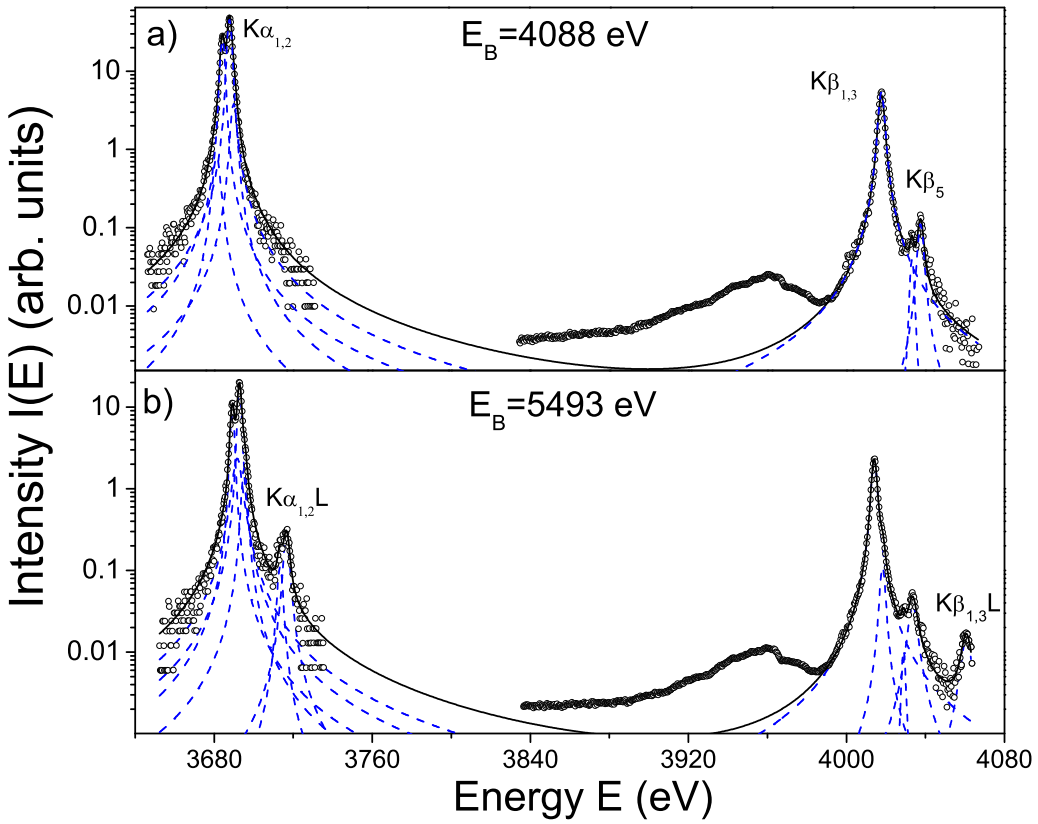

FIG. 3. (Color online) Fitted high-resolution K x-ray spectra of Ca at two different incident-beam energies, (a) E_B=4088 eV and (b) E_B=5493 eV. The solid thick lines represent the total fit to the experimental data (open circles) and the dashed lines the individual fit components. Besides the diagram lines labeled in (a), additional satellite peaks on the high energy sides of the $K\alpha_{1,2}$ and $K\beta_5$ lines correspond to the $K\alpha_{1,2}L$ ($K^{-1}L^{-1}$–L^{-2}) and $K\beta_{1,3}L$ ($K^{-1}L^{-1}$–$M^{-1}L^{-1}$) satellite transitions, respectively. Longer acquisition times were used for the RA region (∼3835 eV-3990 eV), which explains the smaller statistical fluctuations of the normalized data in this part of the spectrum. On the other hand, the "background" region extending from 3735 eV to 3835 eV was skipped.

$K\beta_{1,3}$ yield ratio consistent values of 0.025(7) and 0.030(12) were found from the fits of the spectra acquired at 4088 eV and 5493 eV.

IV. RESULTS AND DISCUSSION

For each beam energy, the total fit to the experimental data was subtracted from the measured x-ray spectrum and the obtained residual spectrum was assumed to correspond to the KMM RA transitions since the RA region was not included in the fits (see Fig. 3). For an easier comparison of the RA transition energies with theory, the residual spectra were shifted in energy, using the centroid of the $K\beta_{1,3}$ peak as the origin of the new energy axis E^R. The shifted residual spectra $Y(E^R)$ corresponding to the two beam energies are depicted in Fig. 4. As shown, the RA intensity is of the order of 10^{-3} relative to the $K\alpha_{1,2}$ diagram lines and of 10^{-2} relative to the $K\beta_{1,3}$ lines. Although the fits of the overall spectra were found to be of good quality with typical reduced chi-squares $\tilde{\chi}^2 \approx 0.999$, the data points in the residual spectra are affected by rather large errors. The latter originate from the statistical errors of the experimental data, the fit errors and the uncertainties related to the data corrections.

A. KMM RA shape

In general, the shapes of the RA spectra measured at the two different excitation energies are very similar and the same onset energies $E_s^R = -22.9(1)$ eV were found for the leading edges of the KMM RA transitions. In the spectrum taken at $E_B = 5493$ eV, however, some structures were found to be less well resolved. As in this case the photon beam energy is higher than the KL double ionization threshold, this can be due to the additional broadening resulting from multi-ionization processes. Furthermore, since both excitation energies are lower than the double K ionization threshold which amounts to 8003 eV for Ca [38], the spectra are free from the $K\alpha_{1,2}^h$ hypersatellite lines appearing in the proton-induced spectra [24] at the energy of -173.5(6) eV. On the other hand, according to [40], for Ca the contributions from the x-ray resonant Raman scattering and RER transitions can be assumed to be negligibly small in comparison with the RA intensity. Therefore the latter contributions were not taken into consideration in the present work.

As mentioned in Sec. I unoccupied nl states in the outer shells are involved in RA SU transitions. In general, one can distinguish four different series of KM_iM_jnl RA transitions, namely the $KM_{2,3}M_{2,3}np$, $KM_1M_{2,3}nd$, $KM_1M_{2,3}ns$ and the KM_1M_1np ones. The RA

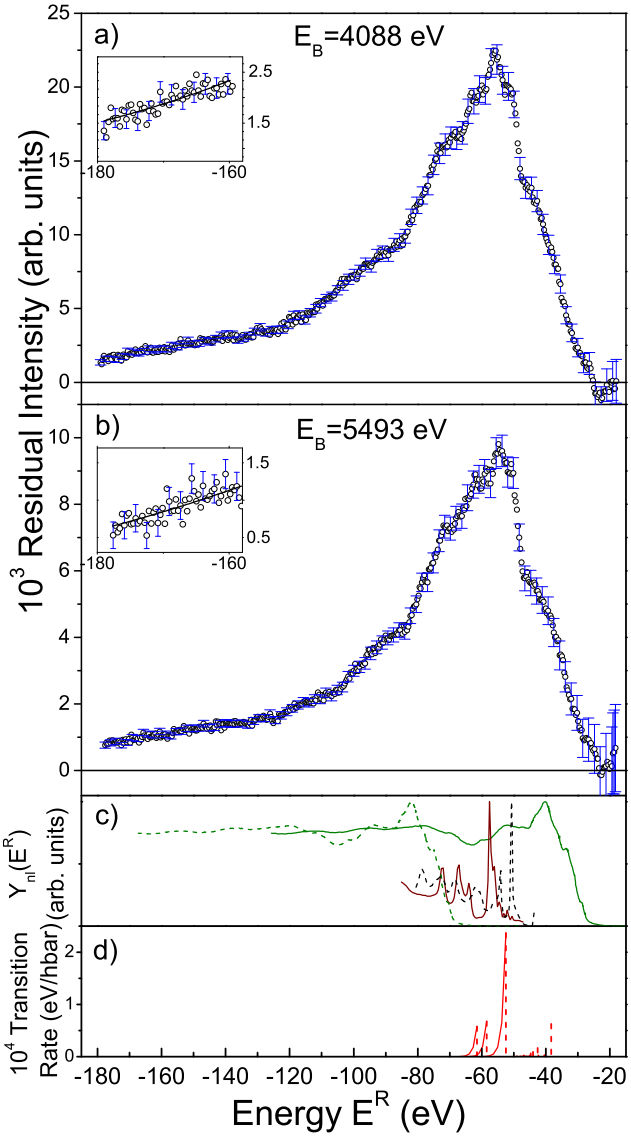

FIG. 4. (Color online) Residual intensities of the fitted high-resolution K x-ray spectra of calcium measured at two beam energies: (a) $E_B = 4088$ eV and (b) $E_B = 5493$ eV. The insets represent the least squares fits (solid lines) of exponential functions to the experimental residuals (open circles) in the lowest 20 eV regions. The fitted exponential functions were used to evaluate the missing RA intensities on the low energy sides. Panel (c) shows the density of unoccupied nl states corresponding to the following RA SU transitions: $3p^{-2}np$ ($n\geq4$) (green solid line), $3s^{-2}np$ ($n\geq4$) (green dashed line), $3s^{-1}3p^{-1}nd$ ($n\geq3$) (black dashed line) and $3s^{-1}3p^{-1}ns$ ($n\geq5$) (wine solid line). In the lowest panel (d), the theoretical radiative field transition rates from Baptista [12] are shown for the $3p^{-2}np$ ($n \geq 4$) RA SU transitions (dotted sticks) and $3p^{-2}\epsilon p$ RA SO transitions (exponential tails).

spectrum should therefore exhibit fine structures reflecting the density of unoccupied states (DOS) as already observed by Kawai *et al.* [5, 6, 41]. Neglecting the quadrupole transitions [42] and the crystal field effects [43], the partial p-like DOS can be derived from the measured K absorption spectrum depicted in Fig. 2. For this purpose, the latter was rescaled relative to the Fermi level energy $E = 4038.2$ eV, which was determined from the first-order derivative of the experimental absorption curve. For the partial s- and d-like DOS, no calculations were found for Ca so that the results of calculations performed for CaS [44] were adopted.

For a meaningful comparison with the measured RA spectrum, the measured absorption spectrum and the normalized nl DOS depicted in the panel (c) of Fig. 4 were set to a common energy scale using the following relation and taking the energy of the $K\beta_{1,3}$ line as reference:

$$Y_{nl}(E^R) = Y_{nl}(E_i - E_{2,3} + E_j - E_{nl}). \tag{10}$$

In the above equation E_i and $E_{2,3}$ are the calcium M_i and $M_{2,3}$ electron binding energies, E_j the binding energy of the outgoing electron calculated within the $Z + 1$ approximation [45] and E_{nl} the energy of the unoccupied nl state. For the binding energies with respect to the Fermi level, values quoted in the X-ray Data Booklet [46] (times -1) were adopted.

As shown in Fig.4 a satisfactory qualitative agreement is observed between the measured RA spectra and the DOS curves. For a more detailed quantitative comparison the leading peaks of the corresponding DOS curves are quoted in the second column of Table I. The first column of the table lists all KMM shake-up RA dipole transitions allowed by the selection rules proposed by Bloch [1] and Aberg [7]. The energies of the corresponding transitions calculated with the DV-$X\alpha$ for solid [10] and radiative field methods for atomic Ca [12] are given in the 3rd and 4th column, respectively. Finally, the RA edge energies derived in [24] from the LMM Auger transition energies reported by Larkins [47] are also listed (5th column).

B. Relative RA yield

The tails of the $K\alpha_{1,2}$ and $K\beta_{1,3}$ diagram lines representing the main source of the background underlying the RA signal, the normalization procedure of the separate spectral regions and the different corrections applied to the measured intensities were checked by comparing the obtained $K\beta_{1,3}$ to $K\alpha_{1,2}$ yield ratios to available theoretical and experimental

TABLE I. The calcium KMM radiative Auger transition energies for different final state configurations relative to the $K\beta_{1,3}$ diagram line (eV). The initial and final atomic states are ^2S and $^2P^o$, respectively. The theoretical energies calculated using the DV-$X\alpha$ [10] and radiative field [12] models as well as the values deduced from the Auger transition energies [24] are also listed for comparison.

KMM-RAE final configuration	EXEFS[a]	DV-$X\alpha$[10]	Radiative field [12]	Transition edge [24]
$3p^{-2}\ ^3P\ 4p$		-41	-38.3	-31.2
$3p^{-2}\ ^1D\ 4p$	-40.1	-43	-40.5	-33.4
$3p^{-2}\ ^1S\ 4p$		-47	-42.3	-35.3
$3p^{-2}\ ^3P\ (n \geq 5)p$		-46	-43.5[b]	
$3p^{-2}\ ^1D\ (n \geq 5)p$		-48	-46.4[b]	
$3p^{-2}\ ^1S\ (n \geq 5)p$		-52	-47.7[b]	
$3s^{-1}3p^{-1}\ ^3P\ 3d$	-50.7	-	-	-48.0[a]
$3s^{-1}3p^{-1}\ ^1P\ 3d$		-	-	
$3s^{-1}3p^{-1}\ ^3P\ (n \geq 4)d$		-	-	
$3s^{-1}3p^{-1}\ ^1P\ (n \geq 4)d$		-	-	
$3s^{-1}3p^{-1}\ ^3P\ 5s$	-57.6	-55	-	-56.7[a]
$3s^{-1}3p^{-1}\ ^1P\ 5s$		-62	-	
$3s^{-1}3p^{-1}\ ^3P\ (n \geq 6)s$		-64	-	
$3s^{-1}3p^{-1}\ ^1P\ (n \geq 6)s$		-71	-	
$3s^{-2}\ ^1S\ 4p$	-81.8	-	-	-73.4
$3s^{-2}\ ^1S\ (n \geq 5)p$		-	-	

[a] Average value for the considered final state configuration.

[b] Average value for the $n \geq 5$ final state configuration.

values (see Table II). It was found that the ratios of 0.098(1) and 0.103(3) obtained for the two beam energies are nearly consistent within the quoted errors. Both are smaller than the theoretical prediction of 0.126 from Scofield [8], but in agreement with the value of 0.107 published later by the same author and with the experimental value of 0.105(5) reported in Ref.[49]. The Lorentzian widths of the $K\beta_{1,3}$ diagram line extracted from the fits of the

TABLE II. Relative $K\beta_{1,3}$ versus $K\alpha_{1,2}$ yields, fitted $K\beta_{1,3}$ Lorentzian widths and measured KMM RA to $K\beta_{1,3}$ intensity ratios for the two incident beam energies.

	Present Results		Results from
	4088 eV	5493 eV	other sources
$I_{K\beta_{1,3}}/I_{K\alpha_{1,2}}$	0.098(1)	0.103(3)	0.126 [8]
			0.107 [48]
			0.105(5) [49]
Lorentzian Width (eV)	2.09(8)	2.22(15)	1.97(17) [36]
R_M	0.055(4)	0.058(5)	0.016(6) [22][a]
			0.031(5) [24][b]
R_c	0.052(4)[c]	0.055(5)[c]	0.056 [8][d]

[a] Experimental value (x-ray tube).
[b] Experimental value (proton beam).
[c] Corrected for the second order $KMMM$ RAE (see text).
[d] Theoretical value (KMN RAE included).

two spectra were also examined. As shown in Table II both results are slightly bigger than the value derived from the atomic level widths recommended by Campbell and Papp [36] but in agreement with the latter within the combined errors. The small surplus found for the experimental Lorentzian widths is due to the unresolved N-satellites which broaden the diagram lines. This explains also why the width observed at 5493 eV is bigger than the one observed at 4088 eV.

The total RA yield was determined by integrating the measured spectra presented in Fig. 4 in the energy interval extending from E_l^R to E_s^R, where E_l^R corresponds to the lowest measured energy of the RA spectrum ($\sim$ -178 eV) and E_s^R to the onset energy of the RA transitions (-21.7 eV). However, as it can be seen from the insets of Fig. 4, at the energy E_l^R the RA intensity is still significantly bigger than zero. The missing RA intensity was evaluated by means of the following relation

$$Y_R = \int_{-E_{K\beta_{1,3}}}^{E_l^R} a_R \exp[b_R E^R]\, dE^R, \tag{11}$$

employing exponential functions to describe analytically the RA x-ray tails according to the

first approximation of the Auger electron escape process [50]. In this equation, a_R and b_R are the least-squares fit parameters to the residuals in the lowest 20 eV energy interval. The fit results are depicted in the insets of Fig. 4. The contribution of this residual part to the measured RA intensity was found to be $\sim 5\%$ and was added to the latter. The total RA intensities were then divided by the corresponding $K\beta_{1,3}$ intensities to get the relative RA yields R_M listed in the 4th row of Table II.

These values were further corrected for the second order $KM-(Mnl)(Mn'l')$ RA process which might slightly contribute to the intensity observed in the low energy region of the KMM RA spectrum. In this process two M Auger electrons and one photon are supposed to be emitted simultaneously. Actually, a similar second order decay channel involving two Auger electrons was already observed in the relaxation of Xe 4d holes [51]. Furthermore, assuming the same value R_c for the first order RA KMM to $K\beta_{1,3}$ and for the second order $KMMM$ to the first order KMM RA yield ratios, the total experimental relative RA yield R_M can be written as

$$R_M = R_c^2 + R_c. \tag{12}$$

The positive solutions of the above equation for R_c yield the final RA relative intensities listed in the last row of Table II. The relative corrections which are smaller than 6% indicate that higher order RA processes have a minor influence.

The difference between the relative KMM RA yields found for the two photon beam energies is not significant, suggesting that the RA intensity does not depend on the excitation energy. Hence, for comparison with other results the average value R_c^{av}=0.053(3) is considered hereafter. One finds first that this average value exceeds markedly the KMM RA to $K\beta_{1,3}$ yield ratios of 0.031(5) and 0.016(6) obtained from measurements performed with proton beams [24] and x-ray tubes [22], respectively. Our result is also underestimated by the theoretical prediction (0.0326) of Baptista [12]. On the other hand, the average RA yield obtained in the present work is close to the the theoretical value of 0.048 obtained by extrapolating the relative RA rates obtained by Åberg for Cl^-, Ar and K^+ [7] and to the total KMM plus KMN relative RA intensity predicted by Scofield (0.0561) [8]. Scofield's prediction ($\sim$0.046) [8, 40, 52] taking into account only $3s$ and $3p$ vacancies in the final states is, however, slightly overerestimated by our experimental value.

In order to get a better overview of the relative KMM RA intensity in the Z region of interest, existing experimental data for Ca and neighboring elements obtained via pho-

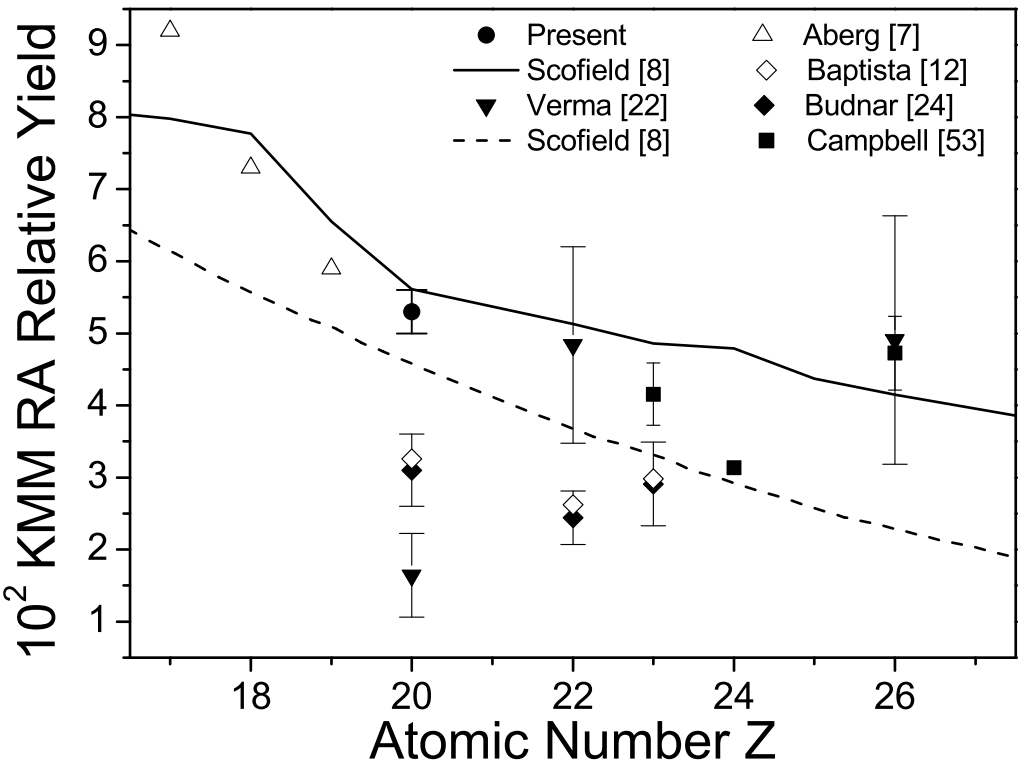

FIG. 5. Present experimental relative KMM RA yield for calcium compared to experimental values from Ref. [24] and Ref. [22] and theoretical values from Scofield for the total KMM + KMN RA transition probabilities (solid line) and only for the KMM ones (dashed line) [8]. Results of calculations for Cl^- (Z=17), Ar (Z=18) and K^+ (Z=19) from [7] and experimental results for the elements V (Z = 23), Cr (Z = 24) and Fe (Z = 26) from [53] are also shown for comparison.

toionization [22, 40, 52], few MeV proton-induced excitation [24] and from measurements of the $K\beta$ to $K\alpha$ intensity ratios in radionuclides following electron capture [53] are plotted in Fig. 5 together with the above mentioned theoretical predictions of Baptista, Åberg and Scofield. First of all we notice a large scattering of the existing experimental data indicating the presence of systematic errors in different experiments. The general decrease with growing atomic numbers predicted by the theory is, however, confirmed by the experiments. No systematic differences between experimental data obtained with different modes of target

ionization are observed. This supports the assumption that the RA x-ray emission does not depend on the primary target excitation. It can be noted also that the present result is the only one obtained so far by using monochromatic synchrotron radiation for the production of the target fluorescence. In addition, present RAE data were collected with an energy resolution of about 1 eV, whereas previous experiments were carried out using either low-resolution energy-dispersive detectors or wavelength-dispersive instruments having a moderate energy resolution of $\sim$ 10 eV. This plays an important role for an accurate determination of the tails of the close-lying $K\alpha_{1,2}$ and $K\beta_{1,3}$ diagram lines since these tails represent the main component of the background underneath the broad RA structure. In our opinion, the main source of the large discrepancies observed between the different experimental RAE data are most probably due to improper background subtractions. Additional RAE measurements for other elements following the method used in the present work are thus clearly needed for more detailed comparisons and more reliable conclusions. Despite the high-energy resolution of the K x-ray spectra measured in the present work, no distinct structures due to shake-up excitations to higher unoccupied outer shells could be observed. This is most likely due to solid state effects which broaden and smear out the discrete RAE structures.

V. SUMMARY AND CONCLUDING REMARKS

Photoinduced KMM radiative Auger emission spectra of Ca were recorded at two different excitation energies. The measurements were performed by means of high-resolution x-ray spectroscopy, using a von Hamos Bragg-type bent crystal spectrometer having an instrumental energy broadening of 1.6 eV. The solid calcium target was irradiated with tunable monochromatic synchrotron radiation beams, which allowed us to selectively exclude the contributions to the RA spectral region from other possible processes such as the x-ray resonant scattering or K hypersatellites. The high energy resolution and the low background characterizing the measured spectra insured a reliable determination of the $K\beta_{1,3}$ diagram line shape. This represented a key point for a correct determination of the weak KMM RA residual yields.

The EXEFS method [5] and DV-X_α [10] calculations were considered to assign properly the structures observed in the RAE spectra. While the experimental transition energies were found to agree well with the results of these two models, the observed RA transition

edges were found to lie systematically above the values derived in [24] from the LLM Auger electron energies reported by Larkins [47]. For the relative yield of the KMM RA with respect to the $K\beta_{1,3}$ diagram line, a value of 0.053(3) was obtained, in good agreement with the theoretical predictions from Scofield [8] and Åberg [7].

Among the few experimental KMM RA relative yields which are available for Ca and neighbouring elements, large discrepancies are found. The latter can be mainly attributed to the difficulties encountered in the accurate determination of the background underlying the RAE spectrum. Due to solid state effects which made the resolution of discrete RAE peaks difficult, we did not attempt to extract separate intensities for the shake-up and shake-off RA transitions. However, the present spectra should allow to do it. For this, however, new theoretical calculations would be very helpful, although such calculations are very challenging for theoreticians due to the complexity of the matrix elements which govern the RA transitions [10].

ACKNOWLEDGMENTS

We wish to acknowledge Dr. R. Tucoulou of the ESRF for the optimal beamline operation during the experiments. The financial supports from the Swiss National Science Foundation (Grant No. 200020-125124), Slovenian Research Agency (Program No. P1-0112) and from the ESRF are acknowledged.

[1] F. Bloch and P. A. Ross, Phys. Rev. **47**, 884 (1935).

[2] F. Bloch, Phys. Rev. **48**, 187 (1935).

[3] T. Åberg and J. Utriainen, Phys. Rev. Lett. **22**, 1346 (1969).

[4] M. O. Krause, T. A. Carlson, , and R. D. Dismukes, Phys. Rev. **170**, 37 (1968).

[5] J. Kawai, T. Nakajima, T. Inoue, H. Adachi, M. Yamaguchi, K. Maeda, and S. Yabuki, Analyst **119**, 601 (1994).

[6] J. Kawai, Analy. Sci. **21**, 733 (2005).

[7] T. Åberg, Phys. Rev. A **4**, 1735 (1971).

[8] J. H. Scofield, Phys. Rev. A **9**, 1041 (1974).

[9] K. G. Dyall and F. P. Larkins, J. Phys. B **15**, 4103 (1982).

[10] H. Hayashi, N. Watanabe, and Y. Udagawa, J. Phys. : Condens. Matter **8**, 37 (1996).

[11] V. O. Kostroun and G. B. Baptista, Phys. Rev. A **14**, 363 (1976).

[12] G. B. Baptista, J. Phys. B : At. Mol. Opt. Phys. **34**, 389 (2001).

[13] K. A. Jamison, J. M. Hall, and P. Richard, J. Phys. B **8**, L458 (1975).

[14] K. A. Jamison, J. M. Hall, J. Oltjen, C. W. Woods, R. L. Kauffman, T. J. Gray, and P. Richard, Phys. Rev. A **14**, 937 (1976).

[15] T. Åberg, K. A. Jamison, and P. Richard, Phys. Rev. A **15**, 172 (1977).

[16] M. Oura, T. Kambara, Y. Kanai, S. Kravis, Y. Nakai, and Y. Awaya, Riken Rev. **4**, 29 (1994).

[17] P.-A. Raboud, M. Berset, J.-Cl. Dousse, Y.-P. Maillard, O. Mauron, J. Hoszowska, M. Polasik, and J. Rzadkiewicz, Phys. Rev. A **65**, 062503 (2002).

[18] J. Hoszowska, A. K. Kheifets, J.-Cl. Dousse, M. Berset, I. Bray, W. Cao, K. Fennane, Y. Kayser, M. Kavčič, J. Szlachetko, and M. Szlachetko, Phys. Rev. Lett. **102**, 073006 (2009).

[19] T. D. Thomas, Phys. Rev. Lett. **52**, 417 (1984).

[20] J. Tulkki and T. Åberg, J. Phys. B **15**, 435 (1982).

[21] C. Herren and J.-Cl. Dousse, Phys. Rev. A **56**, 2750 (1997).

[22] H. R. Verma, J. Phys. B: At. Mol. Opt. Phys. **33**, 3407 (2000).

[23] D. Mitra, M. Sarkar, D. Bhattacharya, and L. Natarajan, X-Ray Spectrom. **37**, 585 (2008).

[24] M. Budnar, A. Mühleisen, M. Hribar, H. Janžekovič, M. Ravnikar, Ž. Šmit, and M. Žitnik, Nucl. Instrum. Methods Phys. Res. B **63**, 377 (1992).

[25] S. P. Limandri, A. C. Carreras, R. D. Bonetto, and J. C. Trincavelli, Phys. Rev. A. **81**, 012504 (2010).

[26] R. D. Deslattes, E. G. Jr. Kessler., P. Indelicato, L. de Billy, E. Lindroth, and J. Anton, Rev. Mod. Phys. **75**, 35 (2003).

[27] J. Hoszowska, J.-Cl. Dousse, J. Kern, and C. Rhême, Nucl. Instrum. Methods Phys. Res. A **376**, 129 (1996).

[28] B. L. Henke, E. M. Gullikson, and J. Davis, At. Data Nucl. Data Tab. **54**, 181 (1993).

[29] W. Jitschin and R. Stötzel, Phys. Rev. A **58**, 1221 (1998).

[30] J. Padežnik-Gomilšek, A. Kodre, I. Arčon, and M. Hribar, Phys. Rev. A **68**, 042505 (2003).

[31] J. R. Janesick, *Scientific Charge-Coupled Devices* (SPIE, Washington, 2001).

[32] J. Szlachetko, J.-Cl. Dousse, J. Hoszowska, M. Berset, W. Cao, M. Szlachetko, and M. Kavčič,

Rev. Sci. Instrum. **78**, 093102 (2007).

[33] M. S. del Río and R. J. Dejus, *Synchrotron Radiation Instrumentation: Eighth International Conference edited by T. Warwick et al.* (Americal Institute of Physics, 2004).

[34] T. Åberg, Phys. Rev. **156**, 35 (1967).

[35] K. G. Dyall, I. P. Grant, C. T. Johnson, F. A. Parpia, and E. P. Plummer, Comput. Phys. Communicat. **55**, 425 (1989).

[36] J. L. Campbell and T. Papp, At. Data Nucl. Data Tab. **77**, 1 (2001).

[37] R. D. Cowan, *The Theory of Atomic Structure and Spectra* (University of California Press, Berkeley, 1981).

[38] M. Oura, H. Yamaoka, K. Kawatsura, K. Takahiro, N. Takeshima, Y. Zou, R. Hutton, S. Ito, Y. Awaya, M. Terasawa, et al., J. Phys. B: At. Mol. Opt. Phys. **35**, 3847 (2002).

[39] M. Deutsch, Phys. Rev. A **39**, 1077 (1989).

[40] O. Keski-Rahkonen and J. Ahopelto, J. Phys. C **13**, 471 (1980).

[41] J. Kawai, Rigaku J. **15**, 33 (1998).

[42] J. J. Rehr and R. C. Albers, Rev. Mod. Phys. **70**, 621 (2000).

[43] F. M. F. de Groot, J. C. Fuggle, B. T. Thole, and G. A. Sawatzky, Phys. Rev. B **41**, 928 (1990).

[44] A. V. Soldatov, A. N. Kravtsova, M. E. Fleet, and X. Liu, Phys. Scripta **T115**, 323 (2005).

[45] M. H. Chen, B. Crasemann, and H. Mark, Phys. Rev. A **21**, 436 (1980).

[46] G. P. Williams, *Electron binding energies: X-ray data booklet compiled and edited by A. C. Thompson and D. Vaughan* (Lawrence Berkeley National Laboratory, 2001).

[47] F. P. Larkins, J. Phys. B: At. Mol. **4**, 1 (1971).

[48] J. H. Scofield, At. Data Nucl. Data Tab. **14**, 121 (1974).

[49] N. V. Rao, S. B. Reddy, G. Satyanarayana, and D. L. Sastry, Physca B+C **138**, 215 (1986).

[50] T. Koshikawa and R. Shimizu, J. Phys. D: Appl. Phys. **7**, 1303 (1974).

[51] P. Lablanquie, S. Sheinerman, F. Penent, R. I. Hall, M. Ahmad, Y. Hikosaka, and K. Ito, Phys. Rev. Lett. **87**, 053001 (2001).

[52] A. Servomaa and O. Keski-Rahkonen, J. Phys. C **8**, 4124 (1975).

[53] J. L. Campbell, A. Perujo, W. J. Teesdale, and B. M. Millman, Phys. Rev. A **33**, 2410 (1986).